Atmos. Chem. Phys., 13, 10505–10516, 2013
www.atmos-chem-phys.net/13/10505/2013/
doi:10.5194/acp-13-10505-2013

Atmospheric Chemistry and Physics Open Access

Atmospheric mercury concentration and chemical speciation at a rural site in Beijing, China: implications of mercury emission sources

L. Zhang[1], S. X. Wang[1,2], L. Wang[1], and J. M. Hao[1,2]

[1]State Key Joint Laboratory of Environment Simulation and Pollution Control, School of Environment, Tsinghua University, Beijing 100084, China
[2]State Environmental Protection Key Laboratory of Sources and Control of Air Pollution Complex, Beijing 100084, China

Correspondence to: S. X. Wang (shxwang@tsinghua.edu.cn)

Received: 26 March 2013 – Published in Atmos. Chem. Phys. Discuss.: 8 May 2013
Revised: 1 September 2013 – Accepted: 16 September 2013 – Published: 30 October 2013

Abstract. Continuous measurements of atmospheric mercury concentration and speciation play a key role in identifying mercury sources and its behavior in the atmosphere. In this study, speciated atmospheric mercury including gaseous elemental mercury (GEM), reactive gaseous mercury (RGM) and particle-bound mercury (PBM) were continuously measured at Miyun, a rural site in Beijing, China, from December 2008 to November 2009. The average GEM, RGM and PBM concentrations were found to be 3.22 ± 1.74, 10.1 ± 18.8 and 98.2 ± 112.7 pg m^{-3}, respectively, about 2–20 times higher than the background concentration of the Northern Hemisphere. The results indicated that atmospheric mercury concentrations in northern China were highly affected by anthropogenic emissions. The atmospheric mercury showed obvious seasonal variations, with the highest seasonal average GEM concentration in summer (3.48 ng m^{-3}) and the lowest value in winter (2.66 ng m^{-3}). In autumn and winter a diurnal variation of GEM was observed, with peak levels in the late afternoon till midnight. Most of the high RGM concentration values occurred in the afternoon of all seasons due to the higher oxidation. The PBM concentration was higher in early morning of all seasons because of the the temperature inversion that increases in depth as the night proceeds. The ratio of GEM to CO indicates that residential boilers play an important role in the elevation of GEM in winter. The ratio of RGM to O_3 could be an indicator of the contribution of local primary sources. The ratio of PBM to $PM_{2.5}$ reveals that the air mass from the east and southwest of the site in spring and summer carries more atmospheric mercury. The HYSPLIT back-trajectory analysis indicated that the monitoring site is affected by local, regional and interregional sources simultaneously during heavy pollution episodes. The results from the potential source contribution function (PSCF) model indicate that the atmospheric transport predominantly from the northwest contributes to the elevated atmospheric mercury in winter and autumn, while the North China Plain (NCP) region and the northern part of the Yangtze River Delta (YRD) region are the major source areas for mercury pollution in spring and summer.

1 Introduction

As it is a global pollutant, great attention has been paid to atmospheric mercury due to its long-range transport and toxicity. Atmospheric mercury can be categorized into total gaseous mercury (TGM) and particle-bound mercury (PBM) in physical form. TGM is further divided into gaseous elemental mercury (GEM) and reactive gaseous mercury (RGM). Schroeder and Munthe (1998) reported that GEM, accounting for over 95 % of TGM, has a long residence time in the atmosphere – from 0.5 to 2 yr. However, based on soil–air exchange fluxes and deposition, Gustin et al. (2008) suggested that the residence time for GEM in the air is on the order of hours to weeks. Atmospheric mercury monitoring is a fundamental approach to understand the atmospheric mercury behavior of one region, and is also used

to identify the local and regional mercury emission sources coupling with back trajectory models.

According to the existing data, the global background concentration of atmospheric mercury is considered to be in the range of 1.5–1.7 ng m^{-3} in the Northern Hemisphere and 1.1–1.3 ng m^{-3} in the Southern Hemisphere (Fu et al., 2012a; Lindberg et al., 2007). Plenty of studies have been conducted in rural areas of the United States since 2000. Sheu et al. (2002) conducted a 1 yr study in Stillpond, Maryland, and found the annual average GEM, RGM and PBM concentration to be 1.7 ± 0.5, 21 ± 22 and 42 ± 50 pg m^{-3}, respectively. Studies conducted in Pompano Beach, Florida (Malcolm et al., 2003), showed similar results for GEM (1.6–2.0 ng m^{-3}) but much lower ranges for both RGM (1.6–4.9 pg m^{-3}) and PBM (0.7–6.3 pg m^{-3}). Lynam and Keeler (2005) reported that the GEM, RGM and PBM concentrations in Dexter, Michigan, were respectively 1.49–1.51, 2–3 and 7–17 pg m^{-3}. The study of Gabriel et al. (2005) on Cove Mountain in Tennessee obtained a GEM average as high as 3.2 ng m^{-3}, and the RGM and PBM concentrations were 16.4 and 9.7 pg m^{-3}, respectively. Five years of monitoring performed in Great Mountain Forest, Connecticut (Sigler and Lee, 2006), showed a GEM range of 1.4–1.6 ng m^{-3}. Similarly, the GEM range of 1.3–1.6 ng m^{-3} was found in Salmon Falls Creek Reservoir, Idaho (Abbott et al., 2007). Valente et al. (2007) reported the GEM, RGM and PBM concentrations to be 1.65, 5 and 7 pg m^{-3}, respectively, in Look Rock, Tennessee. Laurier and Mason (2007) found in Chesapeake Bay Laboratory, Maryland, that the GEM and RGM concentrations were 1.7–1.8 and 6–13 pg m^{-3}, respectively.

China is one of the largest mercury emission sources in the world (AMAP and UNEP, 2008). However, to date, only relatively limited field measurements have been conducted in China to investigate the atmospheric processes of mercury. Most previous studies focused on the urban areas and mining/industrial regions (Fang et al., 2001; Liu et al., 2002; Feng et al., 2004; Wang et al., 2007; Zhu et al., 2012). A few studies were conducted at mountain sites such as Mt. Waliguan, Mt. Gongga and Mt. Changbai (Wang et al., 2007; Fu et al., 2008a, b, 2009, 2010a; Zhu et al., 2008; Wan et al., 2009a, 2009b). There is a lack of mercury monitoring data in rural areas with a regional background for typical heavily polluted regions in China such as the North China Plain (NCP) region. Most of these studies only measured atmospheric mercury, and did not simultaneously observe the concentrations of other air pollutants such as fine particles ($PM_{2.5}$), carbon monoxide (CO) and ozone (O_3), which could help to identify the emission sources and explain the atmospheric behavior of mercury.

In this study, we measured the GEM, RGM and PBM as well as $PM_{2.5}$, CO, and O_3 at a rural site in northern China for a whole year. We analyzed the temporal variation of mercury species, and summarized the correlation between mercury and other air pollutants to investigate the factors affecting its behaviors in the region. Furthermore, based on the NOAA HYSPLIT model and the potential source contribution function (PSCF) model, the potential mercury sources and emission regions were analyzed, which helped to improve the understanding of atmospheric mercury outflow from China.

2 Methodology

2.1 Monitoring site description

The mercury monitoring station (40°28′51″ N, 116°46′30″ E, 220 m a.s.l.) in this study was located in Miyun County, about 100 km northeast to the Beijing urban area (see Fig. 1). Miyun County is famous for its Miyun Reservoir, which is one of the biggest reservoirs in northern China, supplying Beijing residents with fresh water. The surrounding areas within 20 km of the site are largely rural, without large point sources in any direction. Miyun has a temperate continental monsoon climate, which is controlled by the cold Siberian–Mongolian high-pressure system in winter, with the northwest wind dominant; and impacted by the continental low-pressure and Pacific high-pressure systems in summer, with the southeast wind dominant. The mercury emission sources in the Beijing urban area are considered as the local sources for the monitoring station, which is shown in Fig. 1. The mercury emissions from areas of the North China Plain (NCP) region such as Beijing, Tianjin, Hebei, the northern part of Henan and the western part of Shandong are regarded as regional sources for the site. The mercury emissions outside the NCP region are all regarded as the interregional sources for this site.

2.2 Atmospheric mercury monitoring

An automatic atomic fluorescence mercury monitoring system – composed of Tekran™ 2537B, 1130 and 1135 instruments – was employed in this study for measurements of GEM, RGM and PBM (Landis et al., 2002). Although Gustin et al. (2013) and Lyman et al. (2010) expressed that concentrations of reactive mercury (RGM + PBM) measured by the Tekran™ system may be underestimated due to the release of mercury halides from KCl denuders in the presence of ozone, the Tekran™ system is the most accurate instrument system so far, and is widely used for observation of speciated mercury in the ambient air.

The analytical module 2537B uses cold vapor atomic fluorescence spectroscopy (CVAFS) with the detection limit of 0.1 ng m^{-3} (Landis et al., 2002) at the sampling flow rate of 1.0 L min^{-1}. GEM is continuously measured by 2537B every five minutes. The denuder coated with KCl in the 1130 instrument as well as the quartz filter in the 1135 are designed to capture RGM and PBM, respectively. Since there is an impactor at the bottom of the 1130 to remove particles larger than 2.5 μm, PBM in this study is hence referred to as $PBM_{2.5}$, i.e., the mercury on $PM_{2.5}$. The sampling inlet

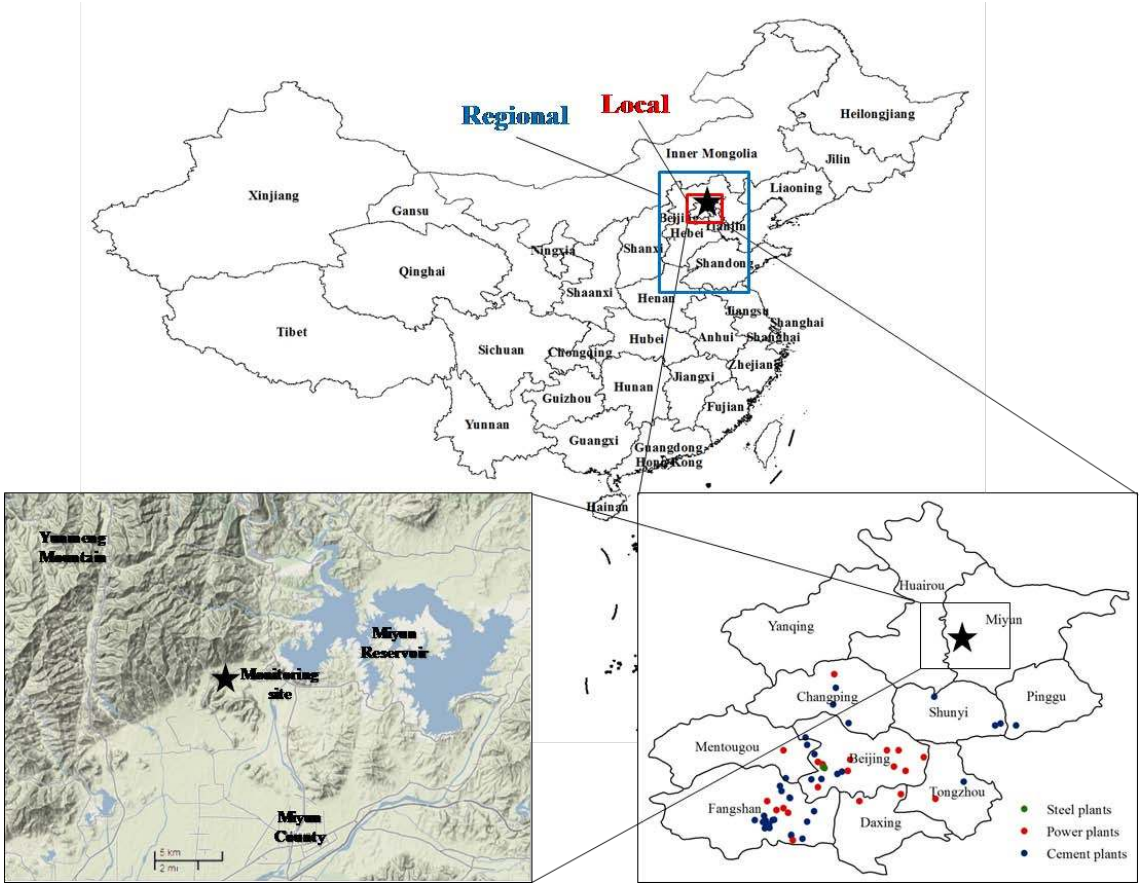

Fig. 1. The location of the Miyun monitoring station in Beijing, China.
Notes: large point sources include power plants, cement plants, and iron and steel plants. Large power plants are defined as those whose installed capacities are larger than 6 MW. Large cement plants are defined as those whose production capacities of cement are larger than 15 kt yr^{-1}. Large iron and steel plants are defined as those whose production capacities of crude steel are larger than 1000 kt yr^{-1}.

is 1.5 m above the instrument platform. Both units are configured to collect 1 h samples at a flow rate of 10 L min^{-1}, resulting in a detection limit of 0.5 pg m^{-3} for RGM and PBM (Landis et al., 2002). After 1h sampling, the quartz filter and the denuder turn to mercury desorption mode in succession at temperatures of 800 and 500 °C, respectively. The 1130 and 1135 systems are flushed with Hg-free air during the next 1 h period, and RGM and PBM are sequentially thermodesorbed and analyzed. The denuder was recoated every two weeks in case of passivation. The 2537B analyzer was calibrated automatically every 25 h using the internal mercury permeation source inside the instrument, and the internal permeation source was calibrated every 6 months with manual injection of mercury by a syringe from an external mercury source (module 2505). Two zero and two span calibrations were performed for each calibration for gold trap A and B, respectively. The error between gold trap A and gold trap B was limited to ±10 %. The impactor plate was changed once every two weeks. The quartz filter was changed once a month. The denuder was recoated once every two weeks following the procedure developed by Landis et al. (2002).

The meteorological parameters such as wind speed, wind direction, air temperature and relative humidity were measured using Vantage Pro2™ weather station (Davis Instruments). CO, O_3 and $PM_{2.5}$ concentrations were also monitored using Thermo Scientific™ model 48i-TLE CO analyzer, model 49i O_3 analyzer and TEOM1405 monitor, respectively. The instrument details are discussed in Wang et al. (2008). All the data were hourly averaged for this study.

2.3 Meteorological data and backward trajectory calculation

The HYSPLIT (Hybrid Single-Particle Lagrangian Integrated Trajectory) model developed by the National Oceanic and Atmospheric Administration (NOAA) is a complete system for computing simple air parcel trajectories to complex dispersion and deposition simulations. In this study, Global Data Assimilation System (GDAS) data with 1° latitude–longitude horizontal resolution was used for source

identification. Back trajectories were calculated for typical pollution events. The total run time was 48 h, which can cover China, Mongolia and eastern Russia. The start time was 04:00 (UTC; note that all times in this paper are UTC.) and restarted every 6 h. The trajectory arrival height was set as 500 m above ground level (a.g.l) to represent the boundary layer where pollutants are usually well mixed.

The potential source contribution function (PSCF) is a useful statistical tool based on the HYSPLIT model to identify source areas for pollutants with a relatively long lifetime such as elemental mercury and CO (Xu and Akhtar, 2010). The PSCF values for mean GEM concentrations in grid cells in a study domain are calculated by counting the trajectory segment endpoints that terminate within each cell. The number of endpoints that fall in the ij-th cell are designated n_{ij}. The number of endpoints for the same cell having arrival times at the sampling site corresponding to GEM concentrations higher than a specific criterion is defined to be m_{ij}. The PSCF value for the ij-th cell is then defined as

$$\mathrm{PSCF}_{ij} = \frac{m_{ij}}{n_{ij}} W_{ij}, \quad (1)$$

where W_{ij} is an empirical weight to reduce the effects of grid cells with small n_{ij} values. In this study, W_{ij} is defined as in the following formula, in which Avg is the mean n_{ij} of all grid cells with n_{ij} greater than zero:

$$W_{ij} = \begin{cases} 1.0 & n_{ij} > 2 \cdot \mathrm{Avg} \\ 0.7 & \mathrm{Avg} < n_{ij} \leq 2 \cdot \mathrm{Avg} \\ 0.42 & 0.5 \cdot \mathrm{Avg} < n_{ij} \leq \mathrm{Avg} \\ 0.17 & n_{ij} \leq 0.5 \cdot \mathrm{Avg}. \end{cases} \quad (2)$$

The PSCF value indicates the probability of a grid cell through which pollution events occurs. More details can be found in the study of Polissar et al. (1999). In this study, the domain that covers the Chinese mainland (73.5–134.5° E, 18.5–53.5° N) is divided into 8450 grid cells with 0.5° × 0.5° resolution. Three-day back trajectories are generated hourly from 1 January to 11 November in 2009 by TrajStat (Wang et al., 2009), a program including HYSPLIT for trajectory calculation with trajectory statistics modules. PSCF maps are plotted using ARCGIS version 9.3.

3 Characteristics of speciated mercury concentration

3.1 General characteristics of speciated mercury in the atmosphere

Speciated mercury concentration data with a 1 yr period from December 2008 to November 2009 was obtained by the Tekran™ mercury monitoring system. The hourly averaged GEM, RGM and PBM concentrations are shown in Fig. 2. The average GEM concentration in Miyun Station is $3.22 \pm 1.74\,\mathrm{ng\,m^{-3}}$, while the concentrations of RGM and PBM are 10.1 ± 18.8 and $98.2 \pm 112.7\,\mathrm{pg\,m^{-3}}$, respectively (see Table 1). GEM accounts for over 95 % of the total mercury concentration. The average total mercury concentration is $3.3\,\mathrm{ng\,m^{-3}}$, about 2 times higher than the background concentration of the Northern Hemisphere (Lindberg et al., 2007). The median value of GEM is 9 % lower than the mean value. The interval of 1st and 3rd quartiles lies in the range of 1.81–4.12 $\mathrm{ng\,m^{-3}}$. However, the mean values of RGM and PBM are much higher than the median values. The mean / median ratios for RGM and PBM are 2.0 and 1.7, respectively. From comparison of the mean values of RGM and PBM with the results from the monitoring sites in rural areas of the US (Valente et al., 2007; Gabriel et al., 2005; Lynam and Keeler, 2005; Malcolm et al., 2003), the RGM concentration of the Miyun site is more or less at the same level as those of US sites. However, the PBM concentration of the Miyun site is much higher than those of US sites, which reflects the severe PM pollution problem in northern China. Table 2 lists the TGM, PBM and RGM concentrations of mercury monitoring sites in China from the existing literature. The TGM concentration of this rural site in Beijing is higher than that of most remote sites, while lower than that of most urban sites. The PBM concentration of this rural site in Beijing is higher than that of all remote sites, while lower than that of all urban sites. The PBM / GEM ratio at Miyun site is higher than most of the monitoring sites in China except the Guiyang urban site, while the RGM / GEM ratio at this site is lower than most of the sites in China except the Mt. Gongga site (see Table 2). This is probably a characteristic of atmospheric mercury in northern China due to the heavy PM pollution. There are several extreme peaks in the observation of the three mercury species. Most of the GEM and PBM peaks match well with the highest air pollution index (API) values in Beijing urban area (shown in Fig. 2), indicating the influence of heavy pollution episodes in Beijing, especially for the period of 3 to 8 November 2009. It should be noted that PM_{10} is the dominant pollutant for Beijing's API during heavy pollution episodes.

3.2 Seasonal variation of speciated mercury concentration

The monthly variation of GEM and the seasonal variation of RGM and PBM are shown in Fig. 3. December–February is considered to be winter, March–May to be spring, June–August to be summer and September–November to be autumn. The highest seasonal average GEM concentration occurs in summer ($3.48\,\mathrm{ng\,m^{-3}}$), while winter has the lowest value ($2.66\,\mathrm{ng\,m^{-3}}$). This is probably due to the long-range transport related to the dominant wind direction, which will be discussed in detail in Sect. 5.2. The dominant wind direction for spring, summer and autumn was southwest, while the wind came mainly from the north and northwest in winter. However, the case of PBM concentration is the opposite. The PBM concentration is higher in winter and lower in summer. The variation range of GEM is relatively larger in spring

Table 1. Statistics of the overall monitoring data and averages during heavy pollution periods for the GEM, RGM and PBM at Miyun, Beijing.

		GEM ($ng\,m^{-3}$)	RGM ($pg\,m^{-3}$)	PBM ($pg\,m^{-3}$)
Statistics	Mean value	3.22	10.06	98.19
	Standard deviation	1.74	18.83	112.72
	Minimum	0.39	0.12	0.49
	1st quartile	1.81	2.59	21.78
	Median (2nd quartile)	2.94	5.02	57.31
	3rd quartile	4.12	10.77	134.48
	Maximum	14.83	301.20	1090.24
Heavy pollution episodes	I: 4–6 May 2009	4.42	4.31	178.37
	II: 12–14 August 2009	3.43	10.92	50.38
	III: 5–7 November 2009	9.69	82.55	373.04

Table 2. Summary of atmospheric speciated mercury concentrations in China.

Location	Classification	Time period	TGM ($ng\,m^{-3}$)	PBM ($pg\,m^{-3}$)	RGM ($pg\,m^{-3}$)	PBM / GEM (10^{-3})	RGM / GEM (10^{-3})	Reference
Guiyang	Urban	Aug 2009–Dec 2009	9.7	368	35.7	38	3.7	Fu et al. (2011)
Shanghai	Urban	Aug 2009–Sep 2009	2.7	–	–	–	–	Friedli et al. (2011)
Nanjing	Urban	Jan 2011–Dec 2011	7.9	–	–	–	–	Zhu et al. (2012)
Ningbo	Urban	Oct 2007–Jan 2008	3.79	–	–	–	–	Nguyen et al. (2011)
Chongqing	Urban	Aug 2006–Sep 2007	6.74	–	–	–	–	Yang et al. (2009)
Changchun	Urban	Jul 1999–Jan 2000	18.4	276	–	15	–	Fang et al. (2004)
Changchun	Rural	Jul 1999–Jan 2000	11.7	109	–	9	–	Fang et al. (2004)
Miyun, Beijing	Rural	Dec 2008–Nov 2009	3.23	98.2	10.1	30	3.1	This study
Chengshantou, Weihai	Remote	Jul 2007–May 2009	2.31	–	–	–	–	Ci et al. (2011a)
Pearl River Delta	Remote	Nov 2008–Dec 2008	2.94	–	–	–	–	Li et al. (2011)
Mt. Changbai	Remote	Aug 2005–Jul 2006	3.58	77	65	22	18.5	Wan et al. (2009a, b)
Mt. Changbai	Remote	Oct 2008–Oct 2010	1.60	–	–	–	–	Fu et al. (2012b)
Mt. Gongga	Remote	May 2005–July 2007	3.98	30.7	6.2	8	1.6	Fu et al. (2008a, b)
Mt. Leigong	Remote	May 2008–May 2009	2.80	–	–	–	–	Fu et al. (2010a)
Mt. Waliguan	Remote	Sep 2007–Aug 2008	1.98	19.4	7.4	10	3.8	Fu et al. (2012c)
Shangri-La	Remote	Nov 2009–Nov 2010	2.59	43.5	8.2	17	3.2	Zhang (2011)
South China Sea	Remote	Aug 2007	2.62	–	–	–	–	Fu et al. (2010b)
Yellow Sea	Remote	Jul 2010	2.61	–	–	–	–	Ci et al. (2011b)

and autumn than that in winter and summer. The variation range of PBM is smaller in summer than other seasons. From winter to autumn, the RGM concentration increases, and the variation range of it becomes larger. RGM is either directly released by anthropogenic sources or formed by the photochemical processes with the oxidation of GEM. The seasonal variation of RGM indicates that the photochemical oxidation processes were more active in summer and autumn than in winter and spring. The heavy pollution episodes in autumn were longer and heavier than those in other seasons due to the disadvantageous diffusion condition, which led to the highest seasonal average RGM concentration in autumn.

3.3 Diurnal variation of speciated mercury concentration

The overall daytime average concentrations of GEM, RGM and PBM were 3.13, 11.5 and 83.6 $pg\,m^{-3}$, respectively, while the overall nighttime averages of the three species were 3.30, 8.7 and 112.0 $pg\,m^{-3}$, respectively. In spring and summer, no significant diurnal variation is found for GEM, as is shown in Fig. 4a. The GEM concentration from late afternoon till midnight (16:00–02:00) is higher than during the rest of the day in autumn and winter. For the RGM concentration in Fig. 4b, most of the high values occur in the afternoon (13:00–15:00) for all four seasons. This is probably related to the intensity of solar radiation. With higher intensity of solar radiation in the afternoon, more GEM is oxidized to RGM. However, the RGM concentration peak for autumn is higher than that for summer, which is due to the disadvantageous diffusion condition in autumn. The PBM concentration, shown in Fig. 4c, is higher in the early morning (01:00–06:00) for all four seasons, which is probably caused by the temperature inversion that increases in depth as the night proceeds. The daily variation of RGM and PBM reflects the formation and removal mechanisms of these two short-lifetime

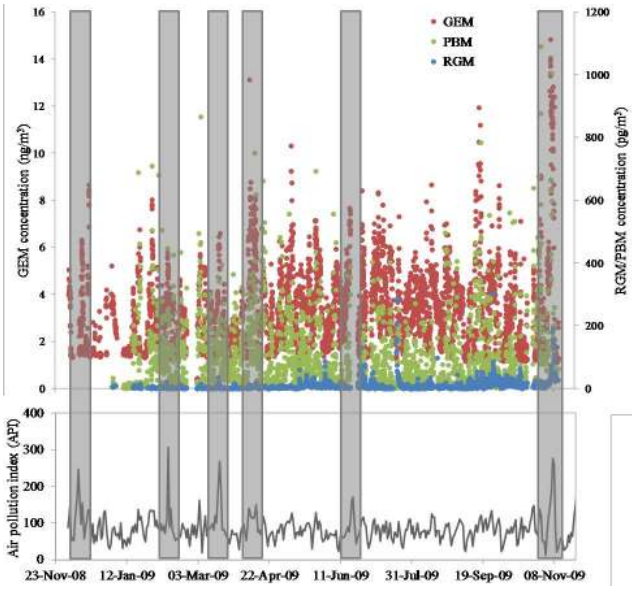

Fig. 2. Hourly averaged GEM, RGM and PBM concentrations at the monitoring site and air pollution index (API) in the Beijing urban area from December 2008 to November 2009.
Notes: the six grey columns are typical heavy pollution episodes in Beijing urban area.

mercury species. Photochemical reaction is the main process for RGM formation, while deposition and adsorption to particles are the two main processes for RGM removal. Adsorption of GEM and RGM to particles is the main process for PBM formation, while rain and dispersion are important processes for PBM removal.

3.4 Correlations between mercury species and meteorological factors

Among all meteorological factors, wind direction has the most significant impact on the concentrations of different mercury species. Figure 5 shows the GEM, RGM and PBM concentrations as well as wind direction frequency in different wind directions. Southwest wind was the dominant wind direction in the monitoring period, with both a high frequency and high wind speed. The high average GEM and PBM concentrations from the southwest direction suggest that the southwest wind brought the most atmospheric mercury pollution to the monitoring site. The influence of wind direction on RGM is not as remarkable as that on GEM and PBM, because RGM is also highly related to other meteorological factors, such as solar radiation. Temperature and relative humidity also has considerable influence on different mercury species with seasonal variations, as shown in Table 3. RGM concentration has a higher dependence on temperature in spring and summer than in autumn and winter, indicating higher RGM formation from photochemical reactions in spring and summer. No correlation was found

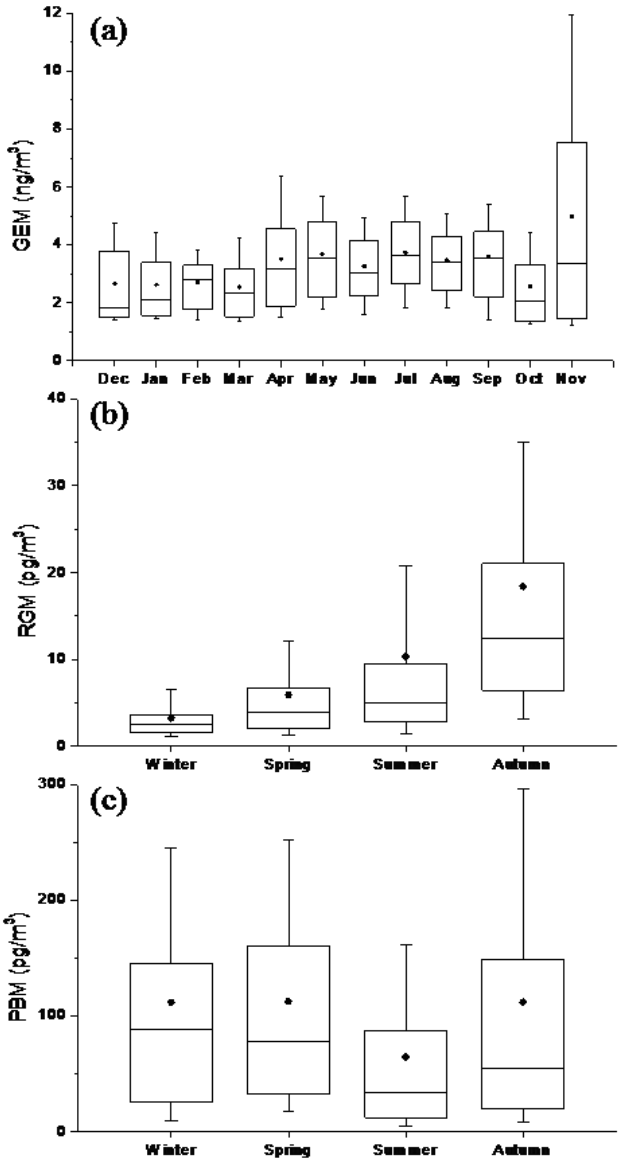

Fig. 3. Monthly variation of **(a)** GEM and seasonal variation of **(b)** RGM and **(c)** PBM concentration. Notes: the bottom and top of the box represent the 25th and 75th percentiles (the lower and upper quartiles), respectively. The band near the middle of the box represents the 50th percentile (the median). The ends of the whiskers represent the 10th and 90th percentiles. The dots represent the mean values.

between temperature and GEM or PBM concentration. The correlations between GEM concentration and relative humidity are notable, with little seasonal variation, which is possibly due to the same pattern of diurnal variation of GEM and relative humidity, i.e., lower in the daytime and higher at night. RGM concentration is positively related to relative humidity in winter, while negatively related in summer. It reveals that moisture in the atmosphere could both scavenge RGM by wet deposition under higher temperature in summer

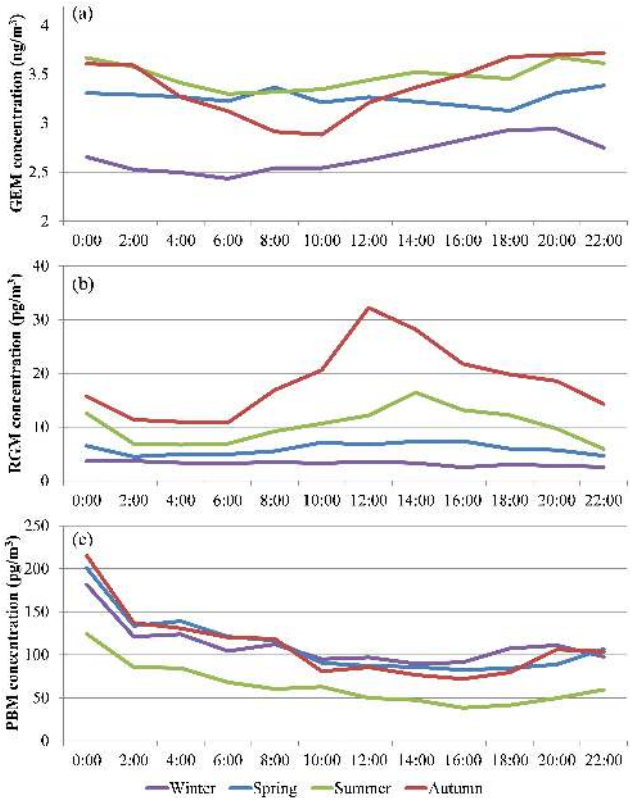

Fig. 4. Daily variation of **(a)** GEM, **(b)** RGM and **(c)** PBM concentration.
Notes: the data were two-hourly averaged.

Table 3. Correlation coefficients between mercury species and meteorological factors in different seasons.

Correlation	Winter	Spring	Summer	Autumn
GEM–temperature	0.21	0.35	−0.06	0.03
RGM–temperature	0.06	**0.45**	**0.46**	−0.01
PBM–temperature	0.07	−0.05	−0.20	−0.13
GEM–relative humidity	**0.47**	**0.46**	**0.48**	**0.48**
RGM–relative humidity	**0.40**	−0.04	**−0.42**	0.04
PBM–relative humidity	**0.51**	**0.44**	0.31	**0.41**

Note: the bold numbers are the ones with higher significance.

and enhance RGM formation by strengthening the oxidation process under lower temperatures in winter. PBM concentration has considerable correlation with relative humidity – it is higher in winter than other seasons. This implies that moisture probably contributes to the formation of PBM, and this influence is amplified under lower temperatures.

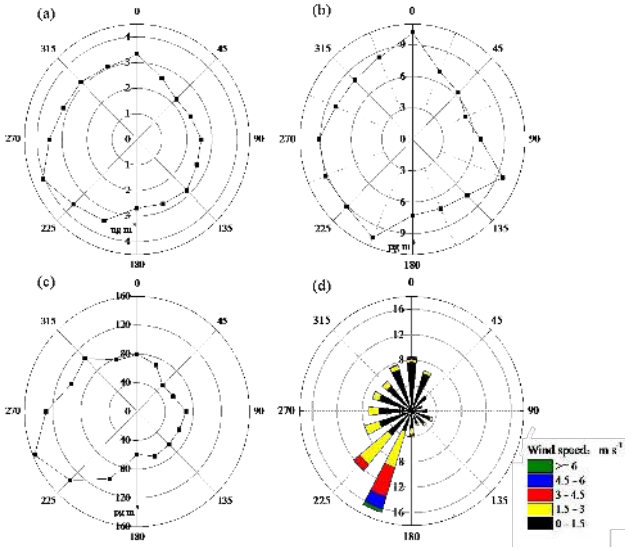

Fig. 5. Statistics of **(a)** average GEM concentration, **(b)** average RGM concentration, **(c)** average PBM concentration and **(d)** wind direction frequency in different wind directions.

4 Mercury source attribution via multi-pollutant correlations

4.1 Source type identification

GEM concentration has a significant correlation with CO concentration due to their homology. Industrial coal combustion, domestic coal combustion, cement production, and iron and steel production are the dominant anthropogenic emission sources for both pollutants (Wu et al., 2006; Wang et al., 2005). Additional to these four types of sources, vehicles are another type of dominant sources for CO, while power plants and nonferrous metal smelters are another two types of dominant sources for GEM. GEM also has a significant natural background, which CO does not. Figure 6 shows the relationship between GEM concentration and CO concentration by season.

The slope of the trend line represents the ratio of GEM emission to CO emission (Hg / CO ratio). For the monitoring station in this study in northern China, the GEM concentration is mainly influenced by coal combustion, including power plants, industrial boilers and residential boilers, while the CO concentration is mainly influenced by coal combustion and vehicles. Nonferrous metal smelters, the second largest anthropogenic source of mercury, are mainly located in the southern part of China, and thus have little influence on the GEM concentration of this station. Based on existing studies (Wang et al., 2005; Wu et al., 2006), the Hg / CO ratio for power plants is larger than that for industrial and residential boilers. In 2001, the Hg / CO ratios for power plants, industrial boilers and residential boilers were 25.2, 2.9 and 0.4, respectively (Wang et al., 2005; Wu et al., 2006). Incomplete

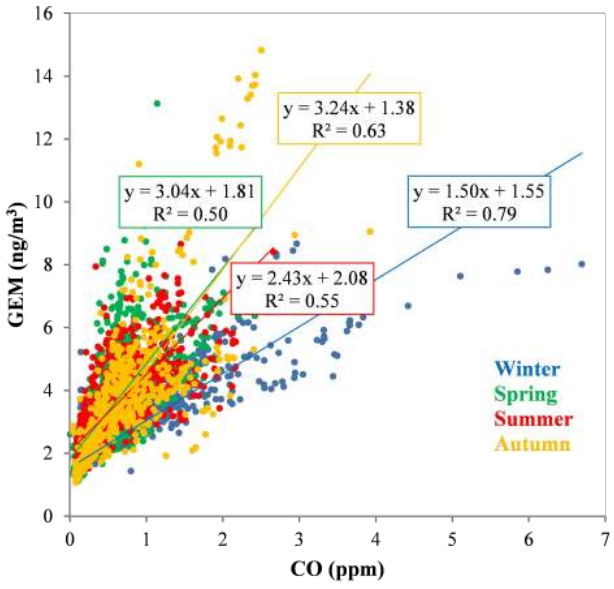

Fig. 6. Correlation between CO concentration and GEM concentration. Notes: The data were hourly averaged.

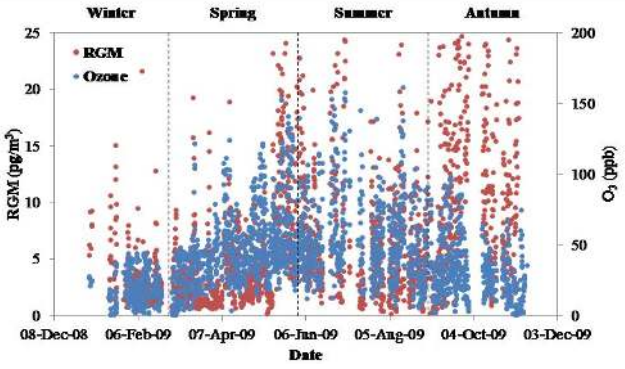

Fig. 7. Comparison of O_3 and RGM concentrations in different seasons.
Notes: the data were hourly averaged.

combustion such as residential coal combustion and biomass burning could lead to a lower Hg / CO ratio. The Hg / CO ratio for vehicles is almost zero. Weiss-Penzias et al. (2007) reported Hg / CO ratios of 5.7, 1.5 and 0.8 for Asian long-range transport (ALRT), Pacific Northwest US biomass burning (BB PNW) and Alaskan biomass burning (BB Alaska), respectively. As shown in Fig. 6, The Hg / CO ratio for winter, spring, summer and autumn are 1.50, 3.04, 2.43 and 3.24, respectively. One of the main causes for the lower Hg / CO ratio in winter could be that the activity level of residential coal combustion is higher in winter. The Hg / CO ratios in Fig. 6 indicate that residential boilers play an important role in mercury pollution in winter.

The intercept of the trend line mainly reflects the intensity of the natural background of GEM. The intercept for summer is higher than that for other seasons because the natural mercury emissions are higher in summer in terms of higher atmospheric temperature. However, the intercept for autumn is lower than that for winter, which is probably due to the heavy GEM pollution episodes. Most of the GEM concentration values higher than 10 ng m^{-3} were from 5 and 6 November 2009, resulting in the counterclockwise rotation of the trend line and thus the decrease of the intercept.

The correlation coefficients of the trend lines for winter, spring, summer and autumn are 0.89, 0.71, 0.74 and 0.79 respectively. The correlation coefficient implies the contribution rate of homological emission sources (e.g., industrial coal combustion, residential coal combustion, cement production, and iron and steel production) to GEM concentration, which fits quite well with the fact that the correlation coefficient for winter is much higher than that for other seasons, because the activity level of coal combustion in northern China is higher in winter for heating supply.

4.2 Impacts of local primary sources

O_3 is a secondary pollutant, and originates from photochemical process; thus it highly depends on the intensity of solar radiation. RGM is formed either directly from local emission sources (i.e., primary RGM) or from the photochemical oxidation of GEM (i.e., secondary RGM). Considering the shorter residence time of both RGM and O_3 compared with GEM, the primary RGM emitted directly from emission sources can be considered as the direct influence of the local sources.

The comparison of O_3 and RGM concentrations in different seasons is shown in Fig. 7. In winter, both the RGM and O_3 were at low levels due to low intensity of solar radiation, while both concentrations were high in summer. The coherence of the variation of RGM and O_3 was high in spring and summer, while low in autumn and winter. This indicates that the monitoring site is more directly influenced by local sources in autumn and winter, while secondary RGM is more important in spring and summer.

After sequencing the RGM / O_3 ratio, the moving correlation coefficients of every 100 pairs of O_3–RGM were calculated. Figure 8 shows the relationship between the moving average RGM / O_3 ratio and the moving O_3–RGM correlation coefficient. It reveals that the O_3–RGM correlation coefficient decreases when the RGM / O_3 ratio increases in the range of 0.05–2 pg m^{-3} ppb^{-1}. This implies that the ratio of RGM to O_3 could be an indicator of local primary sources. A higher RGM / O_3 ratio suggests higher influence from local primary sources. The exceptions outside the common RGM / O_3 ratio range were mainly because the RGM or O_3 concentrations were fairly low (RGM < 1 pg m^{-3}, O_3 < 2 ppb). The peak values of the RGM / O_3 ratio occurred in the period from 3 to 8 November 2009. The back trajectory

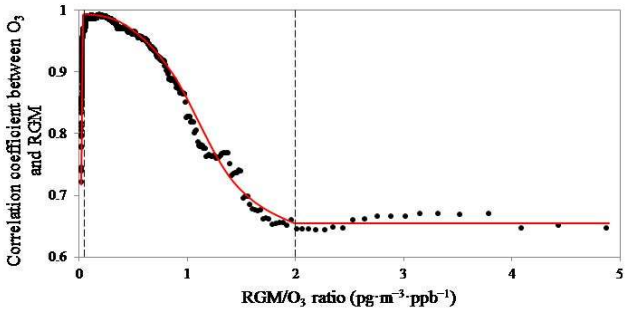

Fig. 8. Relationship between RGM / O_3 ratio and O_3–RGM correlation coefficient.
Notes: the data were hourly averaged.

analysis indicated that this period was mainly influenced by local emission sources, as shown in Sect. 5.1.

4.3 Source direction identification

Relationships between PBM and $PM_{2.5}$ have obvious seasonal variations, as shown in Fig. 9. The slope of the trend line shows the ratio of PBM to $PM_{2.5}$. The ratios for winter, spring, summer and autumn are 2.66×10^{-6}, 3.06×10^{-6}, 3.35×10^{-6} and 2.56×10^{-6}, respectively. Wind direction is a key factor for the variations. Based on the meteorological data, the dominant wind direction for all the four seasons is northeast. However, the subdominant wind directions for spring and summer are east and southwest respectively. The particles from the north mainly originate from sand storms from Inner Mongolia, which is a natural source of particles whose mercury content is low. The particles from the south are mainly from the northern China region, including the Beijing urban area. Most of these particles with high mercury content are emitted from anthropogenic sources, such as coal-fired boilers. Therefore, the slope of the trend line for the relationship between $PM_{2.5}$ and PBM could reveal the mercury source direction. The ratios reveal that the air masses from the east and southwest of the site in spring and summer carry more atmospheric mercury.

5 Mercury source attribution via HYSPLIT modeling

5.1 Identification of mercury sources during heavy pollution episodes

HYSPLIT is a modeling tool to visualize the long-range transport of air mass so as to track the spatial sources of certain pollutants. HYSPLIT modeling was performed for three heavy pollution episodes in spring, summer and autumn – 4–6 May (episode I), 12–14 August (episode II) and 5–7 November (episode III) 2009, respectively – with a runtime of 48 h, shown as Fig. 10. The average GEM, RGM and PBM concentrations for these three episodes are listed in Table 1. The dominant mercury species for the first episode in spring were GEM and PBM, while that for the second episode in summer was RGM. The concentrations of all the three mercury species were significantly high for the third episode in autumn. The air mass in the spring case, episode I, was transported from the Yangtze River Delta (YRD) region to the North China Plain (NCP) region. Almost all of the air mass came from a low atmospheric level with heavy pollution. This is a typical pollution period in spring. The air mass transport in the summer case, episode II, was over a shorter distance than that in the spring case. The air mass in this period originated mainly from southwestern. The air mass in the autumn period, episode III, originated mainly from northwestern. The air mass traveled from the remote northwestern area, where the air was relatively clean, to the Loess Plateau (including part of Gansu, Ningxia, Shanxi and Shaanxi Province), descending from high altitude down to low altitude. The air that originated from the Loess Plateau was mainly at a low atmospheric level, and was carried along with polluted air from urban areas. The three heavy pollution episodes indicate that the monitoring site is affected by local, regional and interregional sources simultaneously. Both the HYSPLIT results and the RGM / O_3 ratios suggest that the mercury pollution in episode I is more impacted by the interregional sources in the YRD region, in episode II it is more impacted by the regional sources in the NCP region, and in episode III it is more impacted by the local sources.

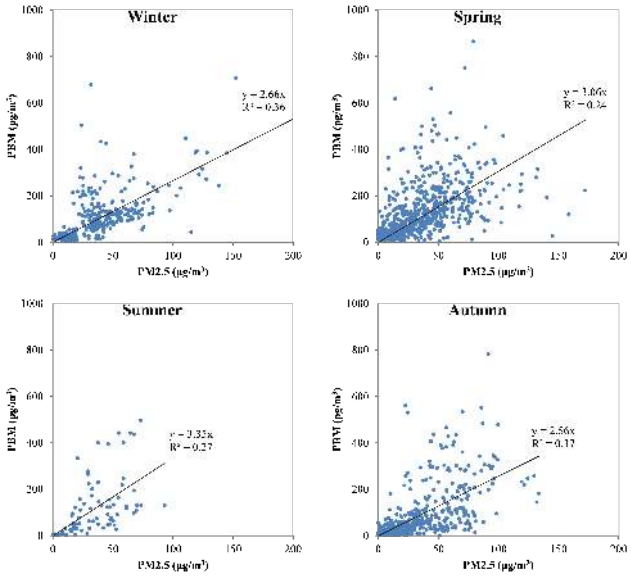

Fig. 9. Relationship between $PM_{2.5}$ and PBM in different seasons.
Notes: the data were hourly averaged.

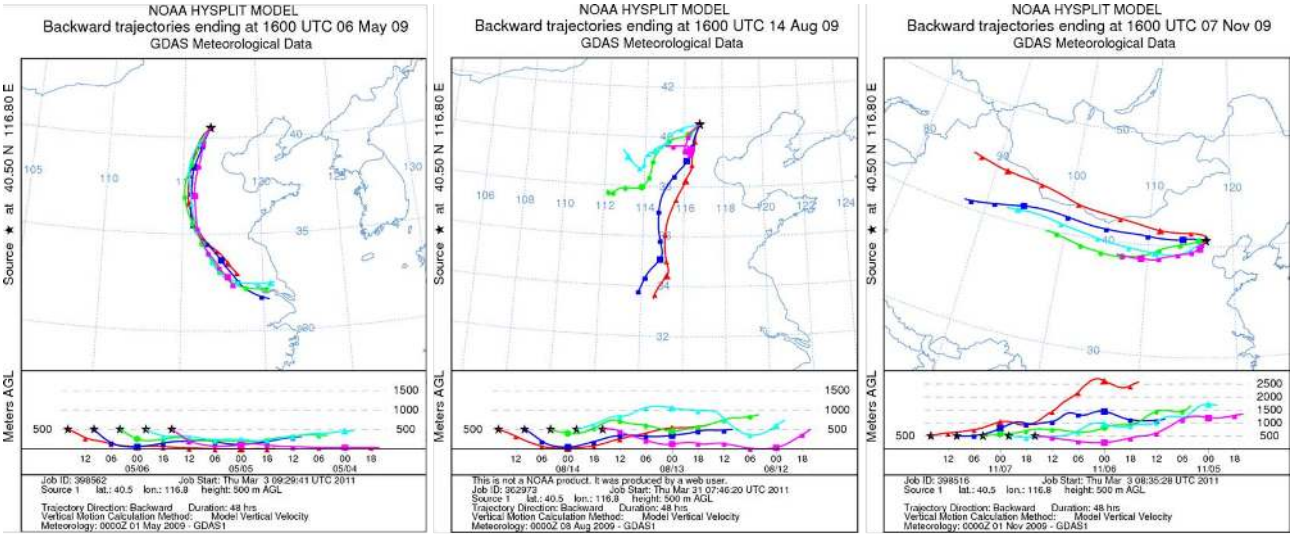

Fig. 10. HYSPLIT modeling results for the periods of **(a)** 4–6 May, **(b)** 12–14 August and **(c)** 5–7 November 2009.

5.2 Spatial distribution of mercury emission sources by PSCF statistics

Influence of the regional or interregional sources can be identified by the PSCF model with the year-round statistics. Figure 11a shows the overall spatial contribution of mercury emission sources in eastern Asia. The NCP region, mainly the part to the south of Beijing, might have significant impacts on the atmospheric mercury distribution pattern at the Miyun monitoring site. The contribution for each season is also given in Fig. 11. In winter and autumn, most of the mercury comes from the remote western and northern areas, including the Loess Plateau and Mongolia. Conversely, the major sources of mercury in spring and summer are located in the areas south and east of Beijing. In summer, especially the provinces of Shandong and Hebei in the NCP region are the two major contributors. In spring, the contributing area expands to Henan, Anhui and Jiangsu, which has reached the north of the YRD region. The year-round statistics indicate that mercury emission in the NCP region is the most important contributor of mercury pollution at the Miyun site. However, it has to be noted that HYSPLIT model has its limitation, and the results could have interference from the "local heavy pollution episodes".

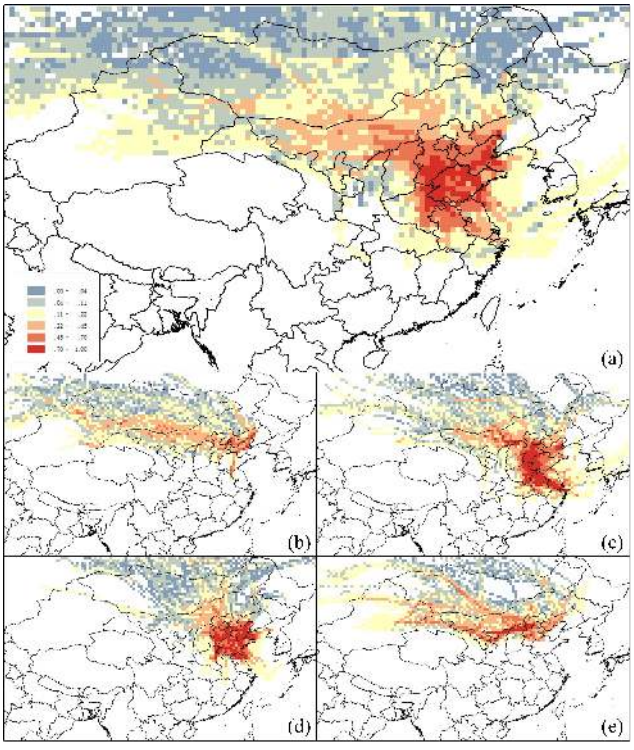

Fig. 11. Spatial contribution of mercury emission sources simulated by PSCF model **(a)** overall, **(b)** winter, **(c)** spring, **(d)** summer, **(e)** autumn.

6 Conclusions

The 1 yr speciated mercury observation in Miyun from December 2008 to November 2009 indicated that the overall average GEM, RGM and PBM concentrations are 3.22 ± 1.74, 10.1 ± 18.8 and 98.2 ± 112.7 pg m^{-3}, respectively. The seasonal average GEM concentration is higher in summer and lower in winter. The PBM concentration, on the other hand, is higher in winter and lower in summer. RGM, formed by the photochemical processes, has a higher concentration and wider range in autumn. No significant daily variation is found

for GEM in spring and summer, while in autumn and winter the GEM concentration from late afternoon till midnight is higher than the rest of the day. Most of the high RGM concentration values occur in the afternoon due to the high intensity of solar radiation. The PBM concentration is higher in the early morning for all four seasons, which is probably related to the temperature inversion that increases in depth as the night proceeds.

GEM concentration has a significant correlation with CO concentration due to their homology. The slope of the trend line represents the ratio of GEM emission to CO emission, which indicates that residential boilers play an important role in the mercury pollution in winter. The intercept of the trend line reflects the intensity of natural background of GEM. The correlation coefficient of GEM and the CO concentration implies the contribution rate of coal combustion to GEM. The ratio of RGM to O_3 could be an indicator of local primary sources. Moreover, the ratio of PBM to $PM_{2.5}$ indicates that the air masses coming from the east and southwest of the site in spring and summer carry more atmospheric mercury.

From the analysis of heavy pollution episodes using the HYSPLIT model, the monitoring site is simultaneously affected by local, regional and interregional sources, and the most heavily polluted episode is more impacted by the local sources. According to the PSCF statistics based on the HYSPLIT model, most of the mercury comes from the remote areas west and north of Beijing, including the Loess Plateau and Mongolia, in autumn and winter. However, the major sources of mercury in spring and summer are located in the areas south and east of Beijing. The transport of mercury emissions from the NCP region to northern part of the YRD region plays a more important role in spring and summer than it does in autumn and winter.

Acknowledgements. This work was sponsored by the Natural Science Foundation of China (No. 20 937002), the Major State Basic Research Development Program of China (973 program) (No. 2013CB430001 & 2013CB430003) and the Collaborative Innovation Center for Regional Environmental Quality. The corresponding author is supported by the Program for New Century Excellent Talents in University (NCET-10-0532). We would like to thank N. Pirrone (CNR, Italy) for his help with the establishment of the Miyun mercury monitoring station, and J. Lin (Larmar University, USA) for his valuable suggestions for this paper.

Edited by: A. Dastoor

References

Abbott, M., Lin, C. J., Martian, P., and Einerson, J.: Atmospheric Mercury Near Salmon Falls Creek Reservoir in Southern Idaho, INL/EXT-06-12048, Idaho Department of Environmental Quality, Boise, Idaho, 2007.

Arctic Monitoring and Assessment Programme (AMAP), and United Nations Environment Programme (UNEP): Technical Background Report to the Global Atmospheric Mercury Assessment, Geneva, Switzerland, 2008.

Ci, Z. J., Zhang, X. S., Wang, Z. W., and Niu, Z. C.: Atmospheric gaseous elemental mercury (GEM) over a coastal/rural site downwind of East China: temporal variation and long-range transport, Atmos. Environ., 45, 2480–2487, 2011a.

Ci, Z. J., Zhang, X. S., Wang, Z. W., Niu, Z. C., Diao, X. Y., and Wang, S. W.: Distribution and air-sea exchange of mercury (Hg) in the Yellow Sea, Atmos. Chem. Phys., 11, 2881–2892, doi:10.5194/acp-11-2881-2011, 2011b.

Fang, F. M., Wang, Q. C., Liu, R. H., Ma, Z. W., and Hao, Q. J.: Atmospheric particulate mercury in Changchun City, China, Atmos. Environ., 35, 4265–4272, 2001.

Fang, F. M., Wang, Q. C., and Li, J. F.: Urban environmental mercury in Changchun, a metropolitan city in Northeastern China: source, cycle, and fate, Sci. Total. Environ., 330, 159–170, 2004.

Feng, X. B., Shang, L. H., Wang, S. F., Tang, S. L., and Zheng, W.: Temporal variation of total gaseous mercury in the air of Guiyang, China, J. Geophys. Res., 109, 3303, doi:10.1029/2003JD004159, 2004.

Friedli, H. R., Arellano Jr., A. F., Geng, F., Cai, C., and Pan, L.: Measurements of atmospheric mercury in Shanghai during September 2009, Atmos. Chem. Phys., 11, 3781–3788, doi:10.5194/acp-11-3781-2011, 2011.

Fu, X. W., Feng, X. B., Zhu, W. Z., Wang, S. F., and Lu, J. L.: Total gaseous mercury concentrations in ambient air in the eastern slope of Mt. Gongga, South-Eastern fringe of the Tibetan plateau, China, Atmos. Environ., 42, 970–979, 2008a.

Fu, X. W., Feng, X. B., Zhu, W. Z., Zheng, W., Wang, S. F., and Lu, J. Y.: Total particulate and reactive gaseous mercury in ambient air on the eastern slope of the Mt. Gongga area, China, Appl. Geochem., 23, 408–418, 2008b.

Fu, X. W., Feng, X. B., Wang, S. F., Rothenberg, S., Shang, L. H., Li, Z. G., and Qiu, G. L.: Temporal and spatial distributions of total gaseous mercury concentrations in ambient air in a mountainous area in southwestern China: Implications for industrial and domestic mercury emissions in remote areas in China, Sci. Total. Environ., 407, 2306–2314, 2009.

Fu, X. W., Feng, X., Dong, Z. Q., Yin, R. S., Wang, J. X., Yang, Z. R., and Zhang, H.: Atmospheric gaseous elemental mercury (GEM) concentrations and mercury depositions at a high-altitude mountain peak in south China, Atmos. Chem. Phys., 10, 2425–2437, doi:10.5194/acp-10-2425-2010, 2010a.

Fu, X. W., Feng, X. B., Zhang, G., Xu, W. H., Li, X. D., Yao, H., Liang, P., Li, J., Sommar, J., Yin, R. S., and Liu, N.: Mercury in the marine boundary layer and seawater of the South China Sea: concentrations, sea/air flux, and implication for land outflow, J. Geophys. Res., 115, 6303, doi:10.1029/2009JD012958, 2010b.

Fu, X. W., Feng, X. B., Qiu, G. L., Shang, L. H., and Zhang, H.: Speicated atmospheric mercury and its potential source in Guiyang, China, Atmos. Environ., 45, 4205–4212, 2011.

Fu, X. W., Feng, X. B., Sommar, J., and Wang, S. F.: A review of studies on atmospheric mercury in China, Sci. Total. Environ., 421–422, 73–81, 2012a.

Fu, X. W., Feng, X., Shang, L. H., Wang, S. F., and Zhang, H.: Two years of measurements of atmospheric total gaseous mercury (TGM) at a remote site in Mt. Changbai area, Northeastern China, Atmos. Chem. Phys., 12, 4215–4226, doi:10.5194/acp-12-4215-2012, 2012b.

Fu, X. W., Feng, X., Liang, P., Deliger, Zhang, H., Ji, J., and Liu, P.: Temporal trend and sources of speciated atmospheric mercury at Waliguan GAW station, Northwestern China, Atmos. Chem. Phys., 12, 1951–1964, doi:10.5194/acp-12-1951-2012, 2012c.

Gabriel, M. C., Williamson, D. G., Brooks, S., and Lindberg, S.: Atmospheric speciation of mercury in two contrasting Southeastern US airsheds, Atmos. Environ., 39, 4947–4958, 2005.

Gustin, M. S., Lindberg, S. E., and Weisberg, P. J.: An update on the natural sources and sinks of atmospheric mercury, Appl. Geochem., 23, 482–493, 2008.

Gustin, M. S., Huang, J. Y., Miller, M. B., Peterson, C., Jaffe, D. A., Ambrose, J., Finley, B. D., Lyman, S. N., Call, K., Talbot, R., Feddersen, D., Mao, H. T., and Lindberg, S. E.: Do we understand what the mercury speciation instruments are actually measuring? Results of RAMIX, Environ. Sci. Technol., 47, 7295–7306, doi:10.1021/es3039104., 2013

Landis, M. S., Stevens, R. K., Schaedlich, F., and Prestbo, E. M.: Development and characterization of an annular denuder methodology for the measurement of divalent inorganic reactive gaseous mercury in ambient air, Environ. Sci. Technol., 36, 3000–3009, 2002.

Laurier, F. and Mason, R.: Mercury concentration and speciation in the coastal and open ocean boundary layer, J. Geophys. Res., 112, 6302, doi:10.1029/2006JD007320, 2007.

Li, Z., Xia, C. H., Wang, X. M., Xia, Y. R., and Xie, Z. Q.: Total gaseous mercury in Pearl River Delta region, China during 2008 winter period, Atmos. Environ., 45, 834–838, 2011.

Lindberg, S., Bullock, R., Ebinghaus, R., Engstrom, D., Feng, X. B., Fitzgerald, W., Pirrone, N., Prestbo, E., and Seigneur, C.: A synthesis of progress and uncertainties in attributing the sources of mercury in deposition, Ambio, 36, 19–32, 2007.

Liu, S. L., Nadim, F., Perkins, C., Carley, R. J., Hoag, G. E., Lin, Y. H., and Chen, L. T.: Atmospheric mercury monitoring survey in Beijing, China, Chemosphere, 48, 97–107, 2002.

Lyman, S. N., Jaffe, D. A., and Gustin, M. S.: Release of mercury halides from KCl denuders in the presence of ozone, Atmos. Chem. Phys., 10, 8197–8204, doi:10.5194/acp-10-8197-2010, 2010.

Lynam, M. and Keeler, G. J.: Artifacts associated with the measurement of particulate mercury in an urban environment: The influence of elevated ozone concentrations, Atmos. Environ., 39, 3081–3088, 2005.

Malcolm, E. G., Keeler, G. J., and Landis, M. S.: The effects of the coastal environment on the atmospheric mercury cycle, J. Geophys. Res., 108, 4357, doi:10.1029/2002JD003084, 2003.

Nguyen, D. L., Kim, J. Y., Shim, S. G., and Zhang, X. S.: Ground and shipboard measurements of atmospheric gaseous elemental mercury over the Yellow Sea region during 2007–2008, Atmos. Environ., 45, 253–260, 2011.

Polissar, A. V., Hopke, P. K., Paatero, P., Kaufmann, Y. J., Hall, D. K., Bodhaine, B. A., Dutton, E. G., and Harris, J. M.: The aerosol at Barrow, Alaska: long-term trends and source locations, Atmos. Environ., 33, 2441–2458, 1999.

Schroeder, W. H. and Munthe, J.: Atmospheric mercury: An overview, Atmos. Environ., 32, 809–822, 1998.

Sheu, G. R., Mason, R. P., and Lawson, N. M.: Speciation and distribution of atmospheric mercury over the northern Chesapeake Bay, ACS Symp. Ser., 806, 223–242, 2002.

Sigler, J. M. and Lee, X.: Recent trends in anthropogenic mercury emission in the northeast United States, J. Geophys. Res., 111, 4316, doi:10.1029/2005JD006814, 2006.

Valente, R. J., Shea, C., Lynn Humes, K., and Tanner, R. L.: Atmospheric mercury in the Great Smoky Mountains compared to regional and global levels, Atmos. Environ., 41, 1861–1873, 2007.

Wan, Q., Feng, X. B., Lu, J. L., Zheng, W., Song, X. J., Han, S. J., and Xu, H.: Atmospheric mercury in Changbai Mountain area, northeastern China I: The seasonal distribution pattern of total gaseous mercury and its potential sources, Environ. Res., 109, 201–206, 2009a.

Wan, Q., Feng, X. B., Lu, J., Zheng, W., Song, X. J., Li, P., Han, S. J., and Xu, H.: Atmospheric mercury in Changbai Mountain area, northeastern China II: The distribution of reactive gaseous mercury and particulate mercury and mercury deposition fluxes, Environ. Res., 109, 721–727, 2009b.

Wang, L. T., Zhang, Q., Hao, J. M., and He, K. B.: Anthropogenic CO emission inventory of Mainland China, Acta. Scientiae. Circumstantiae., 25, 1580–1585, 2005 (in Chinese).

Wang, Y., McElroy, M. B., Munger, J. W., Hao, J., Ma, H., Nielsen, C. P., and Chen, Y.: Variations of O_3 and CO in summertime at a rural site near Beijing, Atmos. Chem. Phys., 8, 6355–6363, doi:10.5194/acp-8-6355-2008, 2008.

Wang, Y. Q., Zhang, X. Y., and Draxler, R.: TrajStat: GIS-based software that uses various trajectory statistical analysis methods to identify potential sources from long-term air pollution measurement data, Environ. Modell. Softw., 24, 938–939, 2009.

Wang, Z. W., Chen, Z. S., Duan, N., and Zhang, X. S.: Gaseous elemental mercury concentration in atmosphere at urban and remote sites in China, J. Environ. Sci., 19, 176–180, 2007.

Weiss-Penzias, P., Jaffe, D., Swartzendruber, P., Hafner, W., Chand, D., and Prestbo, E.: Quantifying Asian and biomass burning sources of mercury using the Hg / CO ratio in pollution plumes observed at the Mount Bachelor observatory, Atmos. Environ., 41, 4366–4379, 2007.

Wu, Y., Wang, S. X., Streets, D. G., Hao, J. M., Chan, M., and Jiang, J. K.: Trends in anthropogenic mercury emissions in China from 1995 to 2003, Environ. Sci. Technol., 40, 5312–5318, 2006.

Xu, X. and Akhtar, U. S.: Identification of potential regional sources of atmospheric total gaseous mercury in Windsor, Ontario, Canada using hybrid receptor modeling, Atmos. Chem. Phys., 10, 7073–7083, doi:10.5194/acp-10-7073-2010, 2010.

Yang, Y. K., Chen, H., and Wang, D. Y.: Spatial and temporal distribution of gaseous elemental mercury in Chongqing, China, Environ. Monit. Assess., 156, 479–489, 2009.

Zhang, H.: Concentrations of speciated atmospheric mercury a high-altitude background station in the Shangri-La area of Tibetan Plateau, China, Abstract to 10th international conference on Mercury as a global pollutant, Halifax, Canada, 2011.

Zhu, J., Wang, T., Talbot, R., Mao, H., Hall, C. B., Yang, X., Fu, C., Zhuang, B., Li, S., Han, Y., and Huang, X.: Characteristics of atmospheric Total Gaseous Mercury (TGM) observed in urban Nanjing, China, Atmos. Chem. Phys., 12, 12103–12118, doi:10.5194/acp-12-12103-2012, 2012.

Zhu, W. Z., Fu, X. W., Feng, X. B., and Lu, J. Y.: Annual time-series analyses of total gaseous mercury measurement and its impact factors on the Gongga Mountains in the southeastern fringe of the Qinghai-Tibetan Plateau, J. Mt. Sci., 5, 17–31, 2008.